Evolution of Temperature Dependence of TRPM2 Channel Gating and Inactivation in Vertebrates

Adam Bartok, Adam V. Toth, and László Csanády *

Department of Biochemistry, *Semmelweis University, Tűzoltó u. 37-47, H-1094 Budapest, Hungary*
HUN-REN-SE Ion Channel Research Group, *Tűzoltó u. 37-47, H-1094 Budapest, Hungary*
HCEMM-SE Molecular Channelopathies Research Group, *Tűzoltó u. 37-47, H-1094 Budapest, Hungary*

Correspondence to László Csanády: Semmelweis University, Department of Biochemistry, Tuzolto u. 37-47, Budapest H-1094, Hungary. *csanady.laszlo@semmelweis.hu (L. Csanády)*
https://doi.org/10.1016/j.jmb.2025.169507
Edited by Lutz Schmitt

Abstract

TRPM2 is a Ca^{2+} permeable cation channel activated by cytosolic Ca^{2+} and ADP ribose (ADPR). In contrast to invertebrate orthologs, vertebrate TRPM2 channels inactivate due to evolutionary alterations in amino acid sequence around the selectivity filter. Human TRPM2 (hsTRPM2) serves as a deep-brain temperature sensor important for body temperature regulation, and its gating is exquisitely temperature dependent. To address whether TRPM2 is temperature sensitive also in ectotherms that lack body temperature regulation, here we investigated the functional properties of zebrafish (*Danio rerio*) TRPM2 (drTRPM2) across the temperature range of 15–37 °C. The rate of ion permeation through the open pore was weakly temperature sensitive ($Q_{10} \sim 1.3$) as expected for a diffusion-limited process. In the presence of saturating concentrations of ligands (ADPR and Ca^{2+}) drTRPM2 open probability showed no temperature dependence. Moreover, for both ADPR and Ca^{2+}, the apparent affinities for channel activation were unaffected by temperature, reporting a standard enthalpy of opening near zero for drTRPM2. Inactivation of drTRPM2 is an order of magnitude slower than that of hsTRPM2. To address whether in both orthologs the same mechanism underlies inactivation, we studied its temperature sensitivity. For both drTRPM2 and hsTRPM2 inactivation rate was modestly temperature dependent ($Q_{10} \sim 2.7$ and ~4.4). A triple substitution which converts the post-filter sequence of drTRPM2 into the corresponding human sequence accelerated drTRPM2 inactivation by 10–20-fold. The data suggest that temperature dependence of hsTRPM2 gating evolved in the course of vertebrate evolution, whereas inactivation was temperature dependent already when it first appeared in early vertebrates.

Introduction

Transient Receptor Potential Melastatin 2 (TRPM2) is a Ca^{2+}-permeable nonselective cation channel activated by binding of cytosolic ADP ribose (ADPR) and Ca^{2+} [1]. In mammals TRPM2 plays important roles in immune cell activation [2], insulin secretion [3]), and the central regulation of body temperature [4,5].

The pore-forming transmembrane domain (TMD) of a homotetrameric TRPM2 channel (structural Layer 1) is formed from six transmembrane helices (S1–S6), and its architecture resembles that of voltage-gated cation channels [6,7]. Within the long extracellular loop that links S5 to S6, a short pore helix followed by a pore loop forms the selectivity filter which largely determines permeation properties [8]. The channel gate is lined by

the C-termini of S6 which form a tetrahelix bundle at the cytosolic membrane surface. In the immediate vicinity of the channel gate, the S2-S3 linkers form highly conserved binding sites for activating Ca^{2+} ions [6,7,9]. Below the TMD, large N- and C-terminal cytosolic regions intertwine to build a three-layered structure (Layers 2–4) which houses two binding sites per subunit for ADPR. A first binding site in Layer 3, formed by an N-terminal domain (N-site) is primarily responsible for channel gating [7,9,10]. A second binding site in Layer 4, formed by the C-terminal NUDT9-homology (NUDT9H) domain (C-site), has adopted different functions in different orthologs: in invertebrate TRPM2 channels it is an active ADPR hydrolase (ADPRase) but plays no role in channel gating [11,12], in vertebrate orthologs it is enzymatically inactive and its role in channel gating is unclear [13]. The structural organization of Layers 1–3 has remained largely conserved from choanoflagellates to man [6,7,9,14].

For all TRPM2 orthologs, channel opening requires simultaneous binding of Ca^{2+} and ADPR, as well as the presence of membrane phosphatidylinositol-4,5-bisphosphate (PIP_2) [11,15,16]. However, whereas invertebrate TRPM2 channels remain active as long as cytosolic ligands are supplied [11], the human channel (hsTRPM2) irreversibly inactivates when kept open by the prolonged presence of agonists [15]. The evolutionary appearance of that inactivation coincided with sequence alterations, between invertebrates and vertebrates, of a specific amino acid triplet in the short helix that follows the selectivity filter ("post-filter helix"): a single-residue deletion and the loss of two negative charges [11]. Replacement of that triplet in the sea anemone (*Nematostella vectensis*) ortholog (nvTRPM2) with the corresponding human doublet induces inactivation in nvTRPM2 [6,11], whereas introduction of the nvTRPM2 triplet into hsTRPM2 eliminates inactivation [6,16]. Inactivation of vertebrate TRPM2 channels thus likely reflects a conformational change of the selectivity filter. Interestingly, for the zebrafish (*Danio rerio*) ortholog (drTRPM2), one of the most ancient vertebrate TRPM2 channels, the rate of inactivation is an order of magnitude slower than for hsTRPM2 [11].

TRPM2 belongs to the subset of TRP channels called "thermoTRPs" for their involvement in temperature sensation [17]. In mammals TRPM2 is expressed in neurons of the thermoregulatory center of the brain, the preoptic area (POA) of the hypothalamus. TRPM2 activity in the POA reports deep-brain temperature, and strongly impacts thermoregulation [4,5]. To achieve that aim, TRPM2 activity must respond to the tiny temperature fluctuations of the brain, typically as small as ±1 °C. Correspondingly, biophysical studies on hsTRPM2 have found its activity to be exquisitely temperature sensitive: intrinsic temperature dependence of gating is greatly enhanced by a positive feedback mechanism caused by Ca^{2+} influx through the open pore. As a result, hsTRPM2 open probability increases by ~2-fold per 1 °C ($Q_{10} \sim 1000$) at physiological ligand concentrations and temperature (~37 °C) [18].

An interesting question is whether temperature-sensitivity was a pre-existing biophysical property of TRPM2 which became exploited in endotherms to employ TRPM2 as a deep-brain thermometer, or whether temperature sensitivity of TRPM2 gating evolved together with the appearance of body temperature regulation. Moreover, although inactivation is also important for shaping TRPM2 activity time courses, its temperature dependence has not yet been studied for any ortholog. We therefore undertook a detailed study of temperature sensitivity of gating and inactivation for TRPM2 from a representative ectothermic early vertebrate. We chose to study drTRPM2 for which a large body of structural and functional information is already available. Previous reports have assessed the properties of other thermoTRPs, such as TRPV1 [19] and TRPA1 [20] expressed in the zebrafish, but for drTRPM2 such detailed studies have not yet been published.

Materials and Methods

Molecular biology

The drTRPM2/pcDNA3.0 construct was generated from drTRPM2/pGEMHE [11] by subcloning the coding region of full-length drTRPM2 (UniProtKB (https://www.uniprot.org) accession number A0A8M3AWC9) into pcDNA3.0. The hum-drTRPM2/pcDNA3.0 construct was generated from drTRPM2/pcDNA3.0 using the QuikChange II XL Site-Directed Mutagenesis Kit (Agilent Technologies). Primers (Forward: CTTCGGCAA CATTCCCGGTTACATTGACAACACCCTGTTCG; Reverse: CGAACAGGGTGTTGTCAATGTAACC GGGAATGTTGCCGAAG) were purchased from Sigma-Aldrich. The construct was confirmed by automated sequencing (LGC Genomics).

Expression of TRPM2 constructs in HEK-293 cells

HEK 293T cells were obtained from ATCC (CRL-11268) and cotransfected with drTRPM2/pcDNA3.0 (or hum-drTRPM2/pcDNA3.0) and GFP/pcDNA3 at a 10:1 ratio (FuGENE HD transfection reagent, Promega). HEK 293 cells stably expressing hsTRPM2 were purchased from SB Drug Discovery. All cells were cultured at 37 °C in 5% CO_2 in DMEM medium supplemented with 4.5 g/L Glucose (Lonza), 10% FBS (EuroClone), 2 mM glutamate, and 100 units/ml penicillin/streptomycin (Lonza).

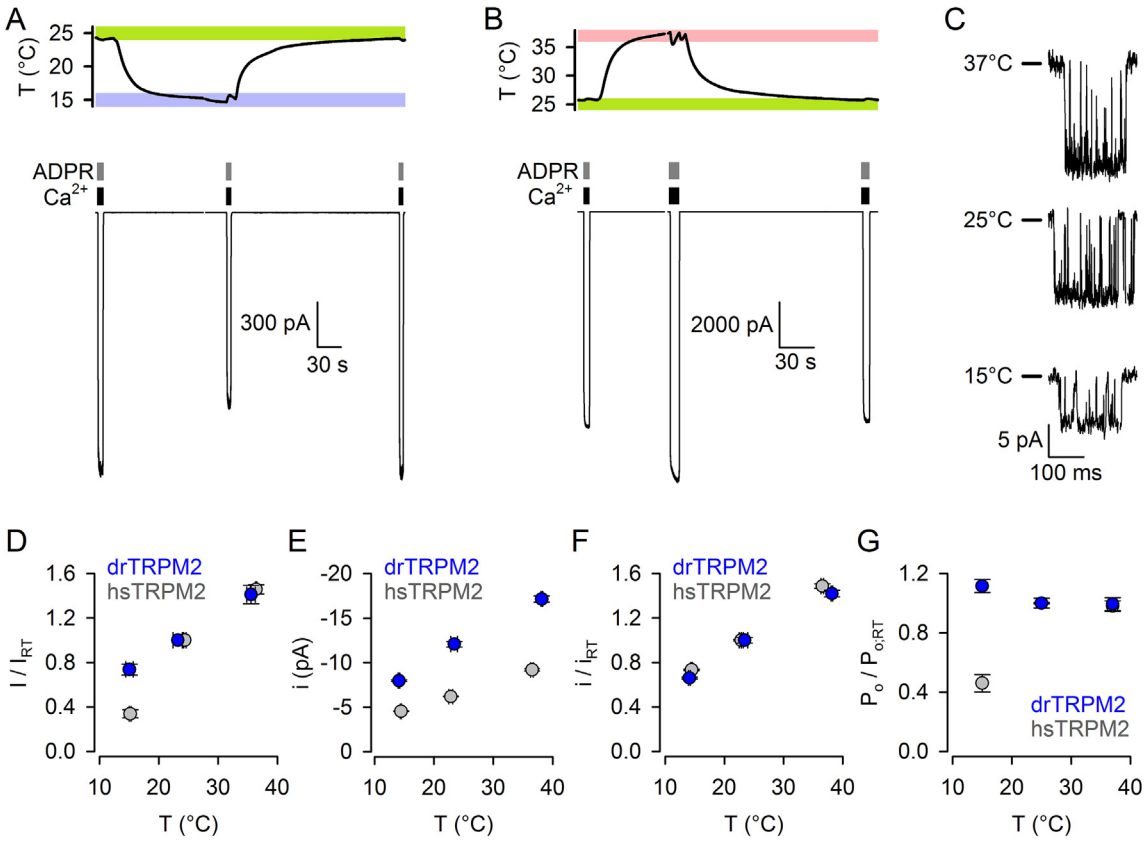

Figure 1. Gating of fully liganded drTRPM2 channels is insensitive to temperature between 15 °C and 37 °C. *(A–B) Bottom*, Macroscopic drTRPM2 currents in inside-out patches from HEK-293T cells evoked by brief exposures to saturating concentrations of cytosolic Ca^{2+} (111–148 μM; *black bars*) and ADPR (32 μM; *gray bars*) at temperatures alternating between ∼25 °C and ∼15 °C (A) or between ∼25 °C and ∼37 °C *(B)*. Membrane potential was −80 mV. Top, Bath temperatures recorded in the immediate vicinity of the patch. *Blue*, *green*, and *rose* boxes highlight target temperature ranges of 15 ± 1 °C, 25 ± 1 °C, and 37 ± 1 °C, respectively. *(C)* Segments of unitary drTRPM2 current at −80 mV at the three target temperatures, obtained as described in Materials and Methods. *(D–G)* Temperature dependence of normalized macroscopic current *(D)*, absolute unitary current amplitude *(E)*, normalized unitary current amplitude *(F)*, and normalized P_o *(G)* for drTRPM2 (*blue symbols*) and hsTRPM2 (*gray symbols*; replotted from [18]). The parameters in panels *D*, *F*, and *G* were normalized to their mean values at ∼25 °C ("RT"). Symbols represent mean ± S.E.M. For drTRPM2 n = 4–6 *(D)* and n = 19–36 *(E–F)*. For hsTRPM2 n = 8–26 *(D)* and n = 4–6 *(E–F)*. In panel G, S.E.M. was calculated from the variances of I/I_{RT} and i/i_{RT} by error propagation.

Inside-out patch-clamp recordings

Currents from drTRPM2 (hum-drTRPM2) or hsTRPM2 channels were recorded in inside-out patches from transiently or stably expressing HEK 293 cells, respectively, as described [18]. Pipette (extracellular) solution contained (in mM) 140 Na-gluconate, 2 Mg-gluconate$_2$, 10 PIPES (pH 7.4 with NaOH at 25 °C) with or without 1 EGTA (pH 7.4 with NaOH at 25 °C). A 140 mM NaCl-based solution for the pipette electrode was carefully layered on top [15]. Bath (cytosolic) solution contained (in mM) 140 Na-gluconate, 2 Mg-gluconate$_2$, 10 PIPES (pH 7.1 with NaOH). Free [Ca^{2+}] in the micromolar range was adjusted by titrating gluconate with Ca^{2+}. For solutions with 1 nM–1 μM free [Ca^{2+}] 1 mM EGTA was added and titrated with Ca^{2+}. Free [Ca^{2+}] was spectrophotometrically determined at each temperature [18]. Temperature dependent changes in pH of the pipette and bath solutions were kept minimal by the use of PIPES buffer (ΔpK_a/10 °C = −0.085). All bath solutions also contained 200 μM AMP (to block endogenous TRPM4-like cation channels) and 10 μM dioctanoyl-PIP$_2$. The bath electrode (in 3 M KCl) was connected to the cytosolic solution through a KCl-agar bridge. The continuously flowing bath solution was exchanged (time constant <100 ms) using electronic valves (ALA-VM8, ALA Scientific Instruments). Flow line temperatures were controlled (TC-10 Dagan Corporation), and bath temperature was continuously monitored (BAT-12, Physitemp) at a distance of ∼2 mm from the membrane patch [21]. Ca^{2+} (Ca-gluconate$_2$; Sigma-Aldrich), ADPR (Sigma-Aldrich), dioctanoyl-PIP$_2$ (Cayman Chemical), and AMP (Sigma-Aldrich) were dissolved into

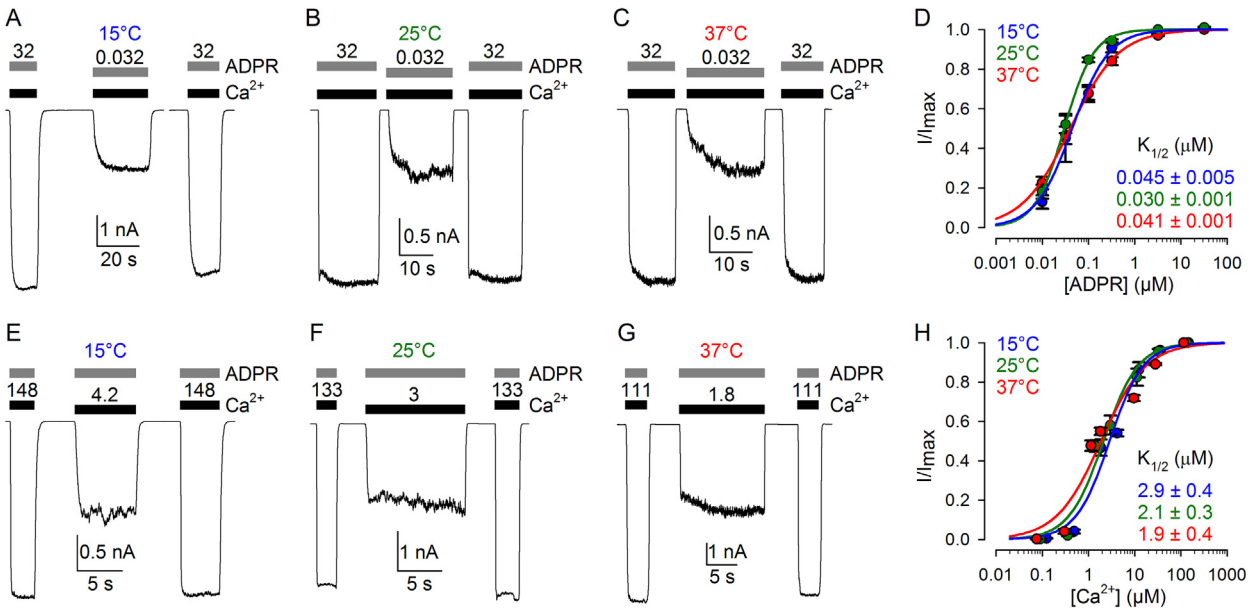

Figure 2. Ligand dose response curves of drTRPM2 are unaffected by temperature. *A–C*, *E–G*, Macroscopic drTRPM2 currents evoked in inside-out patches by alternating brief exposures to saturating and subsaturating concentrations of either ADPR (*A–C*) or Ca^{2+} (*E–G*), together with a saturating concentration of the other ligand. Bath temperature was ~15 °C (*A*, *E*), ~25 °C (*B*, *F*), or ~37 °C (*C*, *G*). Membrane potential was −80 mV. *D*, *H*, Normalized dose response curves for (*D*) ADPR in the presence of saturating Ca^{2+}, and (*H*) for Ca^{2+} in the presence of saturating ADPR, at the three target temperatures (*color coded*). Fractional current in the presence of a test ligand concentration was normalized to the average of the currents evoked in the same patch by bracketed exposures to a saturating ligand concentration. Symbols plot mean ± S.E.M. In *D*, $n = 8–15$ (15 °C), $n = 5–13$ (25 °C), $n = 12–21$ (37 °C). In *H*, $n = 4–9$ (15 °C), $n = 4–8$ (25 °C), $n = 4–11$ (37 °C). *Solid curves* are fits to the Hill equation with midpoints ($K_{1/2}$) plotted in the panels.

the bath solution from >100× concentrated, pH-adjusted aqueous stocks. Currents were recorded at a bandwidth of 2 kHz (Axopatch 200B; Molecular Devices), digitized at 10 kHz (Digidata 1322A; Molecular Devices), and saved to disk (Pclamp10; Molecular Devices).

Data analysis

Macroscopic fractional currents (Figures 1D and 2D, H) were calculated as the mean steady-state current under a test condition (i.e., test concentration of an agonist, or test temperature) normalized to the average of the mean steady-state currents observed in the same patch in bracketing segments of record under reference conditions (i.e., in the presence of maximal agonist concentrations, or at the reference temperature (25 °C)). Dose response curves were fitted to the Hill equation using least squares. Macroscopic current decay time courses were fitted using least-squares to decaying single-exponential functions to obtain time constants (Figures 3B, D, and 4C).

Estimation of unitary current amplitudes

Single-channel current amplitudes were estimated from macroscopic current traces, exploiting the staircase-like current decay caused by channel inactivation (Figure 3A, C). Current amplitude histograms were generated from the section of single-channel current trace provided by the last surviving channel, and fitted by sums of Gaussian functions, and unitary current amplitudes (Figure 1E) estimated as the distances between adjacent peaks.

Statistics

All data are shown as mean ± S.E.M., with the number of independent experiments (n) indicated in the figure legends.

Results

Gating of fully liganded drTRPM2 channels is insensitive to temperature between 15 °C and 37 °C

To study its biophysical properties, drTRPM2 was expressed in HEK-293T cells and studied in excised inside-out patches at −80 mV membrane potential, in symmetrical Na-gluconate based solutions. Macroscopic TRPM2 currents (Figure 1A, B, *Bottom*) and bath temperature in the immediate vicinity of the patch (Figure 1A, B, *Top*) were simultaneously recorded. Continuous direct

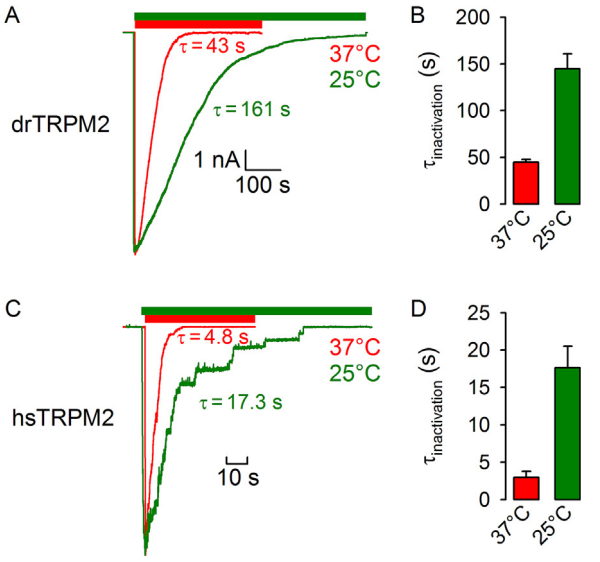

Figure 3. Inactivation rate is temperature dependent for both drTRPM2 and hsTRPM2. *A*, *C*, Macroscopic currents of drTRPM2 (*A*) and hsTRPM2 (*C*) channels in inside-out patches evoked by sustained exposure (*colored bars*) to saturating Ca^{2+} (133–148 μM) plus ADPR (32 μM) at ∼37 °C (*red traces* and *bars*) or ∼25 °C (*green traces* and *bars*). Membrane potential was −80 mV. In *C*, the current traces were rescaled by their maximal amplitudes. *B*, *D*, Time constants of inactivation for drTRPM2 (*B*) and hsTRPM2 (*D*) at ∼ 37 °C (*red*) and ∼25 °C (*green*), obtained from single-exponential fits to the traces in *A*, *C*. Data represent mean ± S.E.M. In *B*, *n* = 39 (37 °C), *n* = 8 (25 °C). In *D*, *n* = 7 (37 °C), *n* = 9 (25 °C).

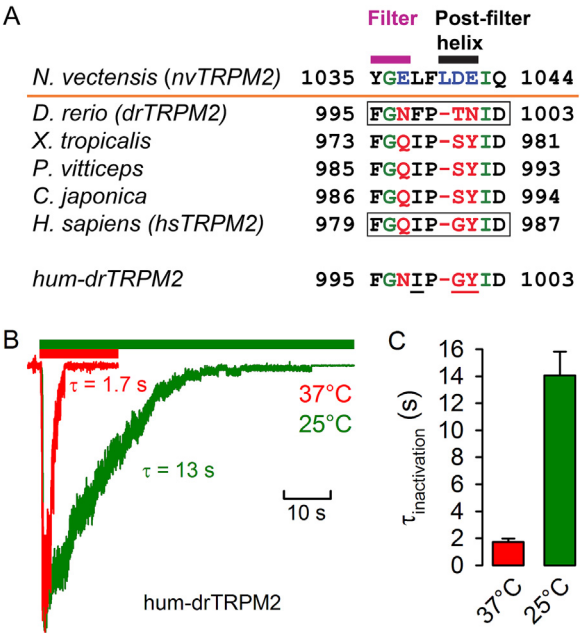

Figure 4. "Humanizing" the drTRPM2 post-filter sequence accelerates inactivation. *A*, Sequence alignment of the filter/post-filter region for nvTRPM2, for representative TRPM2 orthologs from the five vertebrate classes, as well as for the hum-drTRPM2 construct. *Boxes* highlight the drTRPM2 and hsTRPM2 sequences. Residues mutated in hum-drTRPM2 are underlined. *B*, Macroscopic currents of hum-drTRPM2 channels in inside-out patches evoked by sustained exposure (*colored bars*) to saturating Ca^{2+} (133–148 μM) plus ADPR (32 μM) at ∼37 °C (*red trace* and *bar*) or ∼25 °C (*green trace* and *bar*). Current traces were rescaled by their maximal amplitudes. Membrane potential was −80 mV. *C*, Time constants of inactivation of hum-drTRPM2 at ∼37 °C (*red*) and ∼25 °C (*green*). Data represent mean ± S.E.M., *n* = 9 (37 °C), *n* = 11 (25 °C).

superfusion of the cytoplasmic patch surface ensured rapid addition/removal of ligands (Figure 1A, B, *Bottom*, *black* and *gray bars*), and a temperature controller afforded ramping the temperature between our control temperature of ∼25 °C (Figure 1A, B, *Top*, *green boxes*) and either ∼15 °C (Figure 1A, *Top*, *blue box*) or ∼37 °C (Figure 1B, *Top*, *rose box*) (Materials and Methods; [18]).

The slow rate of drTRPM2 inactivation (time constant >100 s at 25 °C; [11]) allowed estimation of macroscopic TRPM2 currents by brief (5–10 s) exposures to saturating concentrations of both Ca^{2+} (111–148 μM, see Materials and Methods) and ADPR (32 μM), without causing substantial inactivation (Figure 1A, B, Bottom). Ligand-activated currents evoked at the test temperatures of ∼15 °C (Figure 1A) or ∼37 °C (Figure 1B) were normalized to the averages of the currents evoked in the same patch in bracketing segments of record at the control temperature of ∼25 °C ("Room Temperature", "RT"). The plot of normalized macroscopic current (I/I_{RT}) vs. temperature (Figure 1D, *blue symbols*) was roughly linear and showed mild temperature dependence. To dissect the contributions of changes in open probability (P_o) and unitary current amplitude (i) to overall temperature sensitivity of drTRPM2 currents, unitary current amplitudes (Figure 1C) were also quantitated (see Materials and Methods) and plotted against temperature, yielding a linear i(T) plot (Figure 1E, *blue symbols*). Although the unitary conductance of drTRPM2 is almost twice as large as that of hsTRPM2 (Figure 1E, *gray symbols*, replotted from [18]), the fractional effect of temperature, obtained by normalizing unitary currents to those at ∼25 °C (i/i_{RT}) was essentially identical for both orthologs (Figure 1F, *blue* vs. *gray symbols*), and consistent with temperature dependence of the rate of diffusion of ions in free solution (Q_{10} ∼ 1.3). The macroscopic current is the product of the unitary current, the open probability, and the number of channels in the patch ($I = i \cdot P_o \cdot N$). Thus, the fractional effect of temperature on open probability ($P_o/P_{o;RT}$) is obtained as $P_o/P_{o;RT} = (I/I_{RT})/(i/i_{RT})$. Whereas for

hsTRPM2 that analysis revealed a marked decline in P_o upon cooling from 25 °C to 15 °C (Figure 1G, *gray symbols*; replotted from [18]), for drTRPM2 (Figure 1G, *blue symbols*) no decline in P_o was detectable. Thus, in contrast to hsTRPM2, for drTRPM2 gating at saturating ligand concentrations shows no temperature dependence between 15 °C and 37 °C.

Apparent affinities of drTRPM2 for ADPR and Ca^{2+} are unaffected by temperature between 15 °C and 37 °C

The apparent lack of temperature dependence of P_o of fully liganded drTRPM2 within the limited temperature span tested here may either reflect a small standard enthalpy of opening (ΔH^0), or may alternatively be caused by a temperature threshold which falls far below the investigated range of temperatures. However, in the latter case temperature dependence should appear at lower, subsaturating ligand concentrations, manifested by rightward shifts in ligand dose–response curves at lower temperatures. E.g., for hsTRPM2 ΔH^0 is large (~180 kJ/mol), but in the presence of saturating ligands the temperature threshold is <15 °C [18], so that P_o is essentially saturated and shows little temperature dependence at $T > 25$ °C (cf., Figure 1G, *gray symbols*). On the other hand, apparent affinities for both ligands decrease by ~5-fold from 40 °C to 25 °C [18].

To differentiate between those two possibilities, ligand concentration dependences of macroscopic current activation were assessed at ~15 °C (Figure 2A, E), ~25 °C (Figure 2B, F), and ~37 °C (Figure 2C, G) for both ADPR (Figure 2A–C) and Ca^{2+} (Figure 2E-G), by normalizing steady-state currents during brief application of a test ligand concentration to the averages of the currents during bracketed applications of a saturating concentration, while keeping the other ligand saturating. The resulting dose response curves (Figure 2D, H; *colored symbols*) were fitted by the Hill equation to obtain apparent $K_{1/2}$ values (Figure 2D, H; *colored curves* and *numbers*). Intriguingly, the dose response curves obtained at the three temperatures essentially overlay with each other for both ADPR and Ca^{2+} – in stark contrast to the large temperature dependent shifts in $K_{1/2}$ reported earlier for hsTRPM2 [18]. These results suggest a virtual lack of temperature dependence, i.e., a small ΔH^0, for the closed-open conformational transition of drTRPM2.

Inactivation rate is modestly temperature dependent for both drTRPM2 and hsTRPM2

Temperature dependence of TRPM2 inactivation has so far not been systematically addressed. We therefore studied the rates of inactivation for both drTRPM2 (Figure 3A) and hsTRPM2 (Figure 3C), by recording macroscopic currents in the prolonged presence of saturating concentrations of both ADPR and Ca^{2+}, at 37 °C (Figure 3A, C; *red traces*) and 25 °C (Figure 3A, C; *green traces*). Inactivation time constants (Figure 3B, D), obtained by single-exponential fits to the current decay time courses, showed significant temperature dependence for both orthologs: compared to 37 °C, the inactivation time constant was prolonged by ~3.2-fold for drTRPM2 ($Q_{10} \sim 2.7$), and by ~6.0-fold for hsTRPM2 ($Q_{10} \sim 4.4$). Thus, inactivation was temperature dependent already when it first appeared in early vertebrates suggesting that – despite the difference in absolute rates between the two orthologs – its mechanism is similar in drTRPM2 and hsTRPM2.

drTRPM2 with a "humanized" post-filter sequence inactivates as fast as hsTRPM2

Following the single-residue deletion and the loss of two negative charges from the post-filter helix, which happened between invertebrates and early vertebrates (Figure 4A, compare *1st* and *2nd row*), three additional substitutions in the post-filter region took place between zebrafish and humans (Figure 4A, compare *boxed sequences*). To address whether the latter substitutions are responsible for the largely accelerated rate of inactivation of hsTRPM2 relative to drTRPM2, a "humanized" drTRPM2 construct ("hum-drTRPM2") was generated by introducing the same three substitutions into drTRPM2 (Figure 4A, *bottom row*). Indeed, inactivation rate of hum-drTRPM2 channels (Figure 4B) was accelerated by ~10–20-fold relative to drTRPM2 and remained temperature dependent (Figure 4C). Thus, both the rate and the temperature sensitivity of inactivation of hum-drTRPM2 became comparable to those of hsTRPM2 (compare Figures 4C to 3D). Of note, although its selectivity filter itself was not fully "humanized" (Figure 4A), the unitary conductance of hum-drTRPM2 also approached that of hsTRPM2: its unitary current amplitude at −80 mV membrane potential was −8.3 ± 0.1 pA at 37 °C ($n = 14$) and −5.7 ± 0.1 pA at 25 °C (compare to Figure 1E, *gray symbols*).

Discussion

Zebrafish body temperature adopts its environmental temperature, which ranges from ~10 °C to ~40 °C in various natural habitats of this species [22]. In the present study we compared functional properties (conductance, gating, and inactivation) of drTRPM2 across most of that temperature range.

We found that gating of drTRPM2 lacks temperature dependence ($\Delta H^0 \sim 0$), in contrast to the strong intrinsic temperature dependence of hsTRPM2 gating ($\Delta H^0 \sim 180$ kJ/mol; [18]). This

finding is intriguing, given that the gating mechanisms of the two orthologs are otherwise very similar, both being activated by ligand binding to structurally highly conserved binding sites: Ca^{2+} binding to the S2-S3 linker and high-affinity ADPR binding to the N-site [7,9,13,23–25]. Moreover, even the conformational rearrangements observed upon ligand binding are similar, at least for structural Layers 1–3 [7,9]. We show here that for drTRPM2 apparent $K_{1/2}$ values for both ligands are tuned to be similar to those reported for hsTRPM2 at 40 °C [18], ensuring high-affinity activation of the zebrafish channel across the entire temperature range encountered by this species.

From a biophysical point of view, an interesting question is which structural parts of hsTRPM2 are responsible for its temperature sensitivity. In that regard, the various thermoTRP channels appear to employ diverse sets of mechanisms. For the close homolog TRPM4 which shares, from a functional point of view, Ca^{2+}-activation and, from a structural point of view, Layers 1–3 with TRPM2, temperature sensitivity has been proposed to result from a "temperature-sensitive Ca^{2+} binding site" in the N-terminal cytosolic region, distinct from the conventional Ca^{2+} site formed by the TMDs [26]. However, because the Ca^{2+}-coordinating side chains of that cytosolic Ca^{2+} site are not conserved in TRPM2, it seems unlikely that the mechanism proposed to underly TRPM4 temperature dependence would also apply to TRPM2. One structural difference between drTRPM2 and hsTRPM2 is the arrangement of Layer 4 in the unliganded state. Due to intersubunit interactions between the N-terminal region and a short segment (the "P-loop") of the unliganded NUDT9H domain, unliganded Layer 4 forms a closed gating ring in hsTRPM2, but not in drTRPM2 which lacks a P-loop [7,9]. Indeed, it has been suggested that the NUDT9H P-loop of hsTRPM2 does play a role in its temperature sensitivity [27]. However, to confound the picture, the P-loop is also present in TRPM2 orthologs of other ectothermic vertebrates (amphibians and reptiles) and even of more ancient species such as cartilaginous fishes and invertebrates, suggesting that it was selectively deleted in bony fishes. Thus, detailed biophysical studies on the structural organization and temperature dependence of more TRPM2 orthologs will be required to shed light on the actual role played by the P-loop, and on the exact structural underpinnings of hsTRPM2 temperature sensitivity.

TRPM2 inactivation, which appeared in early vertebrates, reflects pore instability due to a triple substitution in the outer pore ([6,11,16], Figure 4A). Here we show that further acceleration of that process in hsTRPM2 is caused by additional substitutions in the same region (Figure 4B). The modest temperature dependence of that process is unlikely to be physiologically relevant for TRPM2 expressed in the human brain, where the temperature is maintained within a narrow range of 1–3 °C. In contrast, it might potentially play a physiological role in zebrafish, the body temperature of which adopts a large range (>30 °C) of environmental temperatures.

Zebrafish are responsive to environmental temperature gradients [19], which implies the ability to sense temperature. Of note, temperature dependent RNA editing has been implicated in temperature adaptation of the octopus [28], and is present also in the zebrafish [29]. However, in contrast to molluscans, in the zebrafish most editing events happen in non-coding regions; the small number of editing events identified in coding regions do not affect any thermoTRP channel gene [29]. From a physiological point of view, a question of interest is which thermoTRP channels contribute to temperature sensing in the zebrafish. Such a role has already been demonstrated for drTRPV1 [19] and for one of two drTRPA1 paralogs [20,30]. Future studies will need to address whether drTRPM2, which is expressed in various populations of sensory neurons during different stages of zebrafish development [31], contributes to temperature sensing at all. In principle, the temperature dependence of its inactivation might become relevant at extreme environmental temperatures.

Supported by EU Horizon 2020 Research and Innovation Program grant 739593, and National Research, Development and Innovation Fund grants KKP 144199 and TKP2021-EGA-24 to L.C. and ADVANCED 149640 to A.B. A.B. was supported by the János Bolyai Research Scholarship of the Hungarian Academy of Sciences (BO/00103/20 and BO/00238/25/8) and the New National Excellence Program (ÚNKP) Bolyai + scholarship of the Ministry of Human Capacities of Hungary (ÚNKP-20-5-SE-6, ÚNKP-21-5-SE-10 and ÚNKP-22-5-SE-12). A.V.T. was supported by the 2024-2.1.1-EKÖP-2024-00004 University Research Scholarship Programme of the Ministry for Culture and Innovation of Hungary (source National Research, Development and Innovation Fund).

CRediT authorship contribution statement

Adam Bartok: Writing – original draft, Visualization, Methodology, Investigation, Funding acquisition, Formal analysis, Data curation, Conceptualization. **Adam V. Toth:** Investigation, Funding acquisition. **László Csanády:** Writing – original draft, Visualization, Methodology, Funding acquisition, Formal analysis, Data curation, Conceptualization.

DATA AVAILABILITY

All data generated over the course of this study are included within the paper.

DECLARATION OF COMPETING INTEREST

The authors declare that they have no known competing financial interests or personal relationships that could have appeared to influence the work reported in this paper.

Received 22 July 2025;
Accepted 21 October 2025;
Available online 24 October 2025

Keywords:
transient receptor potential;
thermoTRP;
endothermic;
ectothermic;
temperature sensing

References

[1]. Perraud, A.L., Fleig, A., Dunn, C.A., Bagley, L.A., Launay, P., Schmitz, C., Stokes, A.J., Zhu, Q., Bessman, M.J., Penner, R., Kinet, J.P., Scharenberg, A.M., (2001). ADP-ribose gating of the calcium-permeable LTRPC2 channel revealed by Nudix motif homology. *Nature* **411**, 595–599.

[2]. Yamamoto, S., Shimizu, S., Kiyonaka, S., Takahashi, N., Wajima, T., Hara, Y., Negoro, T., Hiroi, T., Kiuchi, Y., Okada, T., Kaneko, S., Lange, I., Fleig, A., Penner, R., Nishi, M., Takeshima, H., Mori, Y., (2008). TRPM2-mediated Ca^{2+} influx induces chemokine production in monocytes that aggravates inflammatory neutrophil infiltration. *Nature Med.* **14**, 738–747.

[3]. Uchida, K., Dezaki, K., Damdindorj, B., Inada, H., Shiuchi, T., Mori, Y., Yada, T., Minokoshi, Y., Tominaga, M., (2011). Lack of TRPM2 impaired insulin secretion and glucose metabolisms in mice. *Diabetes* **60**, 119–126.

[4]. Song, K., Wang, H., Kamm, G.B., Pohle, J., Reis, F.C., Heppenstall, P., Wende, H., Siemens, J., (2016). The TRPM2 channel is a hypothalamic heat sensor that limits fever and can drive hypothermia. *Science* **353**, 1393–1398.

[5]. Kamm, G.B., Boffi, J.C., Zuza, K., Nencini, S., Campos, J., Schrenk-Siemens, K., Sonntag, I., KabaoÄŸlu, B., El Hay, M.Y.A., Schwarz, Y., Tappe-Theodor, A., Bruns, D., Acuna, C., Kuner, T., Siemens, J., (2021). A synaptic temperature sensor for body cooling. *Neuron* **109**, 3283–3297.

[6]. Zhang, Z., Tóth, B., Szollosi, A., Chen, J., Csanády, L., (2018). Structure of a TRPM2 channel in complex with Ca (2+) explains unique gating regulation. *Elife* **7**, e36409.

[7]. Huang, Y., Roth, B., Lu, W., Du, J., (2019). Ligand recognition and gating mechanism through three ligand-binding sites of human TRPM2 channel. *Elife* **8**, e50175.

[8]. Schnitzler, M., Waring, J., Gudermann, T., Chubanov, V., (2008). Evolutionary determinants of divergent calcium selectivity of TRPM channels. *FASEB J.* **22**, 1540–1551.

[9]. Huang, Y., Winkler, P.A., Sun, W., Lu, W., Du, J., (2018). Architecture of the TRPM2 channel and its activation mechanism by ADP-ribose and calcium. *Nature* **562**, 145–149.

[10]. Kuhn, F.J., Kuhn, C., Winking, M., Hoffmann, D.C., Luckhoff, A., (2016). ADP-ribose activates the TRPM2 channel from the sea anemone *Nematostella vectensis* independently of the NUDT9H domain. *PLoS One* **11**, e0158060.

[11]. Iordanov, I., Tóth, B., Szollosi, A., Csanády, L., (2019). Enzyme activity and selectivity filter stability of ancient TRPM2 channels were simultaneously lost in early vertebrates. *Elife* **8**, e44556.

[12]. Tóth, B., Iordanov, I., Csanády, L., (2020). Selective profiling of N- and C-terminal nucleotide-binding sites in a TRPM2 channel. *J. Gen. Physiol.* **152**, e201912533.

[13]. Iordanov, I., Mihályi, C., Tóth, B., Csanády, L., (2016). The proposed channel-enzyme transient receptor potential melastatin 2 does not possess ADP ribose hydrolase activity. *Elife* **5**, e17600.

[14]. Huang, Y., Kumar, S., Lee, J., Lu, W., Du, J., (2024). Coupling enzymatic activity and gating in an ancient TRPM chanzyme and its molecular evolution. *Nature Struct. Mol. Biol.*.

[15]. Csanády, L., Torocsik, B., (2009). Four Ca2+ ions activate TRPM2 channels by binding in deep crevices near the pore but intracellularly of the gate. *J. Gen. Physiol.* **133**, 189–203.

[16]. Tóth, B., Csanády, L., (2012). Pore collapse underlies irreversible inactivation of TRPM2 cation channel currents. *PNAS* **109**, 13440–13445.

[17]. Hilton, J.K., Rath, P., Helsell, C.V., Beckstein, O., Van Horn, W.D., (2015). Understanding thermosensitive transient receptor potential channels as versatile polymodal cellular sensors. *Biochemistry* **54**, 2401–2413.

[18]. Bartók, Á., Csanády, L., (2022). Dual amplification strategy turns TRPM2 channels into supersensitive central heat detectors. *PNAS* **119**, e2212378119.

[19]. Gau, P., Poon, J., Ufret-Vincenty, C., Snelson, C.D., Gordon, S.E., Raible, D.W., Dhaka, A., (2013). The zebrafish ortholog of TRPV1 is required for heat-induced locomotion. *J. Neurosci.* **33**, 5249–5260.

[20]. Oda, M., Kurogi, M., Kubo, Y., Saitoh, O., (2016). Sensitivities of two zebrafish TRPA1 paralogs to chemical and thermal stimuli analyzed in heterologous expression systems. *Chem. Sens.* **41**, 261–272.

[21]. Toth, A.V., Bartok, A., (2025). Direct assessment of temperature sensitivity of the TRPM2 channel with the patch clamp technique. *Methods Mol. Biol.* **2908**, 163–170.

[22]. Aleström, P., D'Angelo, L., Midtlyng, P.J., Schorderet, D. F., Schulte-Merker, S., Sohm, F., Warner, S., (2020). Zebrafish: housing and husbandry recommendations. *Lab Anim.* **54**, 213–224.

[23]. Tóth, B., Iordanov, I., Csanády, L., (2014). Putative chanzyme activity of TRPM2 cation channel is unrelated to pore gating. *PNAS* **111**, 16949–16954.

[24]. Kuhn, F.J.P., Ehrlich, W., Barth, D., Kuhn, C., Luckhoff, A., (2019). Functional importance of NUDT9H domain and N-terminal ADPR-binding pocket in two species variants of vertebrate TRPM2 channels. *Sci. Rep.* **9**, 19224.

[25]. Wang, L., Fu, T.M., Zhou, Y., Xia, S., Greka, A., Wu, H., (2018). Structures and gating mechanism of human TRPM2. *Science* **362** pii: eaav4809.

[26]. Hu, J., Park, S.J., Walter, T., Orozco, I.J., O'Dea, G., Ye, X., Du, J., Lã, W., (2024). Physiological temperature drives TRPM4 ligand recognition and gating. *Nature* **630**, 509–515.

[27]. Gattkowski, E., Johnsen, A., Bauche, A., Möckl, F., Kulow, F., Garcia, A.M., Rutherford, T.J., Fliegert, R., Tidow, H., (2019). Novel CaM-binding motif in its NudT9H domain contributes to temperature sensitivity of TRPM2. *Biochim. Biophys. Acta, Mol. Cell Res.* **1866**, 1162–1170.

[28]. Birk, M.A., Liscovitch-Brauer, N., Dominguez, M.J., McNeme, S., Yue, Y., Hoff, J.D., Twersky, I., Verhey, K. J., Sutton, R.B., Eisenberg, E., Rosenthal, J.J.C., (2023). Temperature-dependent RNA editing in octopus extensively recodes the neural proteome. *Cell* **186**, 2544–2555.

[29]. Li, W., Bu, M., Hu, R., Jiang, S., Chen, L., Somero, G.N., (2023). Tissue-specific temperature dependence of RNA editing levels in zebrafish. *BMC Biol.* **21**, 262.

[30]. Prober, D.A., Zimmerman, S., Myers, B.R., McDermott Jr., B.M., Kim, S.H., Caron, S., Rihel, J., Solnica-Krezel, L., Julius, D., Hudspeth, A.J., Schier, A.F., (2008). Zebrafish TRPA1 channels are required for chemosensation but not for thermosensation or mechanosensory hair cell function. *J. Neurosci.* **28**, 10102–10110.

[31]. Kastenhuber, E., Gesemann, M., Mickoleit, M., Neuhauss, S.C., (2013). Phylogenetic analysis and expression of zebrafish transient receptor potential melastatin family genes. *Dev. Dyn.* **242**, 1236–1249.